




Designing Co-based microwave absorber with high absorption and thin thickness based on structure regulations

Xiaomin Wu^{1,2}, Yonglin Yao^{1,2,*} , Youqi Fan¹, Zhuo Zhao¹, and Jing Zhan³

¹Anhui Province Key Laboratory of Metallurgical Engineering & Resources Recycling, Anhui University of Technology, Maanshan 243002, China

²School of Metallurgical Engineering, Anhui University of Technology, Maanshan 243032, China

³School of Metallurgy and Environment, Central South University, Changsha 410083, China

Received: 26 June 2021

Accepted: 12 October 2021

Published online:
23 October 2021

© The Author(s), under exclusive licence to Springer Science+Business Media, LLC, part of Springer Nature 2021

ABSTRACT

Two strategies were employed to improve the microwave absorbing property of Co powders by constructing special structures in this paper. In the first way, the Co powder with a network structure was prepared through a simple immersion–calcination method by using corncobs as templates. This network structure contributes to enhanced dielectric loss, magnetic loss, and optimized impedance matching, and so the Co network exhibits an excellent microwave absorbing property. At the sample thickness of 2.34 mm, the reflection loss reaches up to – 54.74 dB, and the effective absorbing bandwidth is 3.20 GHz. What is more, the Co network shows strong and broadband absorption at small thicknesses. The reflection loss reaches – 30.80 dB at 14.16 GHz when the sample thickness is 1.35 mm, while the effective absorbing bandwidth is up to 5.36 GHz (12.64–18 GHz) at the sample thickness of 1.45 mm. In the second way, the Co@C network with a core–shell structure was constructed. However, unlike most of the reported magnetic/carbon composites, the introduced carbon layer played a negative role, due to the decreased loss capability and deteriorated impedance matching. Therefore, the Co powder with strong absorption, wide absorbing band, and thin thickness was obtained just by constructing a network structure, and it can be used as a promising microwave absorber.

Address correspondence to E-mail: yaoyonglin@ahut.edu.cn

1 Relevance summary

1. The Co powders with a network structure were prepared by using corncobs as templates. This network structure contributes to enhanced dielectric loss, magnetic loss, and optimized impedance matching, and so the Co network exhibits excellent microwave absorbing properties at thin thicknesses.

2. The Co@C network with a core–shell structure was prepared. However, compared with the reported literatures, the carbon shell has an abnormal effect on the microwave absorbing property, and the reason was analyzed.

3. Two new criteria considering the effects of sample thickness were proposed to evaluate the microwave absorbing property.

2 Introduction

In the last several decades, increasingly severe environmental pollution has attracted world-wide concern. Different from some traditional chemical pollution, such as water pollution [1], air pollution [2], and solid waste pollution [3, 4], electromagnetic pollution including electromagnetic interference (EMI) and electromagnetic radiation (EMR) is a new kind of physical pollution [5]. The EMI and EMR can influence the normal operation of precision instruments, and cause serious damage to people's health [6–8]. In order to solve the electromagnetic pollution problem, two strategies, i.e., electromagnetic shielding and electromagnetic absorption were usually employed [9]. In these two methods, electromagnetic absorbing materials play an important role because they can eliminate the incident electromagnetic wave radically by converting it to thermal energy. In addition, due to the pressing needs of military equipment, microwave absorbing materials have become the key of stealth technique. Therefore, in recent years, more and more attention has been paid to the preparation of new microwave absorbers with strong absorption, wide bandwidth, light weight, and thin thickness [10, 11].

Dielectric loss and magnetic loss are the two main loss ways for microwave absorbing materials. Therefore, the microwave absorption performance of a material mainly depends on its dielectric and magnetic properties. Among various microwave

absorbers, magnetic metal powders generally possess both high dielectric loss and strong magnetic loss. In addition, due to the high Snoek's limit, magnetic metal powders can still maintain excellent magnetic properties at high frequencies, which is unattainable for another often used magnetic material—ferrites [12]. Therefore, magnetic metal powders were considered to be promising microwave absorbing materials. Up to now, a large number of magnetic metal powders, such as Fe [13], Co [14, 15], Ni [16], FeNi [17, 18], FeCo [19, 20], and NiCo [21] powders have been prepared, and enhanced microwave absorption was obtained by adjusting their morphologies, structures, or compositions. However, for most magnetic metal powders, the magnetic loss is much stronger than dielectric loss [22, 23], which would deteriorate the impedance matching between absorbers and free space, and then lead to most of the incident microwaves reflected on the absorbers' surfaces. Therefore, the magnetic metal powder absorbers usually suffer from high thickness and narrow absorbing bandwidth, which restricted their practical application [24]. Up to now, it is still a challenge to optimize the microwave absorbing properties of magnetic metal powders and improve their practicability.

Among the common magnetic metals, cobalt is more stable than Fe, and has larger saturation magnetization than Ni. Therefore, up to now, various Co-based microwave absorbing materials have been studied [25, 26]. In this paper, we developed two strategies which are hopeful to optimize the microwave absorbing property of Co powders. First, the Co powder with a network structure was prepared by using corncobs as templates. The network structure can form a conductive network and enhance the electron conduction, and further improve the dielectric loss by the enhanced conduction loss [27]. Second, the Co@C network with a core–shell structure was constructed by coating a carbon layer on the Co network. It is well known that carbon is an excellent dielectric material. A large number of carbon-based materials have been synthesized and they exhibited outstanding microwave absorbing properties [28–30]. Recently, the combination of various carbon and magnetic materials has become the main tendency of microwave absorbing materials [31–35]. Therefore, both the network structure and the carbon shell may be helpful to balance the magnetic loss and dielectric loss of Co powders, and then optimize the impedance

matching. Based on the above structural design, a new Co-based microwave absorber with strong absorption, wide bandwidth, light weight, and thin thickness is expectable.

3 Experimental

3.1 Preparation of Co and Co@C networks

The preparation route of the Co and Co@C networks are illustrated in Fig. 1. First, 0.5 g spongy cores of corncobs were submerged in 50 mL $\text{Co}(\text{NO}_3)_2$ ethanol solution (0.8 mol L^{-1}) for 5 h under room temperature. Second, the spongy cores adsorbed Co^{2+} were calcined at $700 \text{ }^\circ\text{C}$ for 2 h in air atmosphere, and then at $500 \text{ }^\circ\text{C}$ for 1 h in a mixed atmosphere (volume ratio, $\text{Ar}:\text{H}_2 = 1:1$). Through these two calcination processes, the corncobs can be burnt out and the absorbed Co^{2+} will form a Co network.

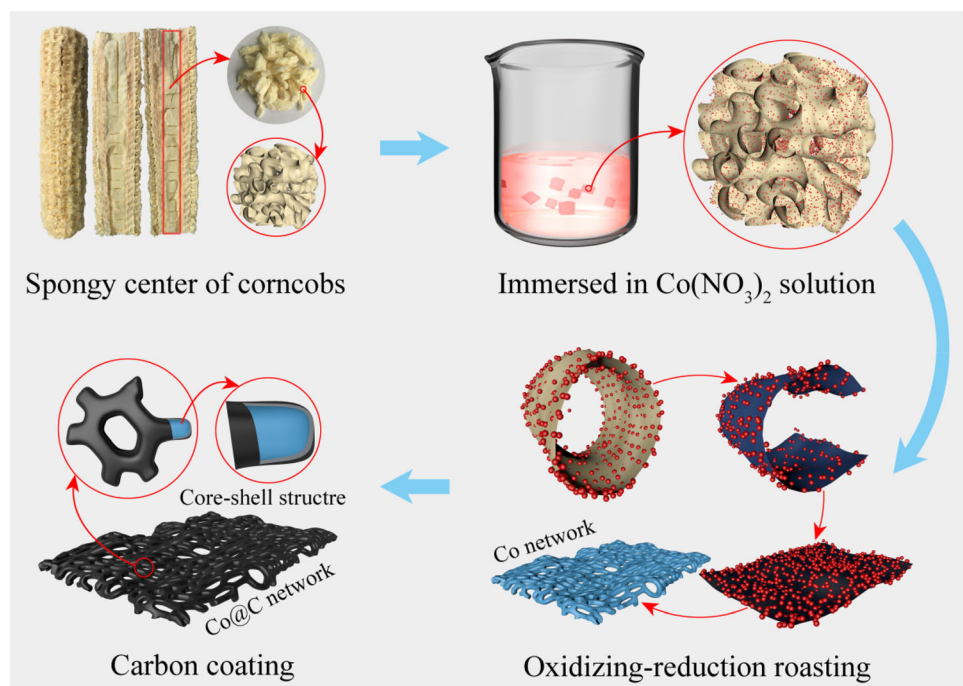
Hydrothermal and solvothermal techniques have many advantages, for example, the morphology and size of particles can be easily controlled. Therefore, they were widely used for the preparation of various nanoparticles [36, 37]. Here, the Co network was coated with a carbon layer through a simple one-step hydrothermal process by using glucose as carbon sources. In this hydrothermal procedure, 0.2 g as-prepared Co network was first dispersed in 40 mL

glucose solution (0.5 mol L^{-1}), and then the solution was maintained at $180 \text{ }^\circ\text{C}$ for 10 h in a Teflon-lined autoclave. When the autoclave was cooled to room temperature naturally, the prepared Co@C composite powders were separated by a magnet, washed with water and ethanol for three times, and dried at $50 \text{ }^\circ\text{C}$ for 4 h in a vacuum oven. At last, the Co@C powders were thermally treated at $500 \text{ }^\circ\text{C}$ for 2 h in a N_2 atmosphere for the further carbonization of the carbon layer.

3.2 Characterization

The phase structures of the prepared Co and Co@C powders were characterized by a X-ray diffractometer (XRD, D8 Advance, Bruker, German) under $\text{CuK}\alpha$ radiation. The carbon was determined by Raman spectrum which was carried out on a laser Raman spectrometer (inVia, Renishaw, UK) at laser excitation of 532 nm. X-ray photoelectron spectroscopy (XPS) was employed to determine the composition of the elements through a multifunctional imaging electron spectrometer (Thermo ESCALAB 250XI, USA). The micro morphologies and structures of the powders were observed by a field emission scanning electron microscope (FESEM, NANO SEM430, FEI, USA) and a transmission electron microscope (TEM, JEM-2100, JEOL, Japan). The magnetic properties of

Fig. 1 Illustration of the preparation route of the Co and Co@C networks



the powders were measured by a magnetic property measurement system (MPMS, XL, Quantum Design, USA). The thermal behavior of the powders under air atmosphere was characterized by an thermogravimetric–differential thermal analyzer (TG–DTA, DTG-60H, Shimadzu, Japan) at a scan rate of $10\text{ }^{\circ}\text{C min}^{-1}$ from room temperature to $650\text{ }^{\circ}\text{C}$.

3.3 Evaluation of microwave absorbing properties

The electromagnetic parameters (relative complex permittivity and permeability) in 2–18 GHz of the samples were measured by a vector network analyzer (Agilent E5071C). For this measurement, the Co or Co@C powders (30 wt %) were first homogeneously mixed with a certain amount of paraffin, and then the mixtures were compressed into coaxial rings with thickness, inner diameter, and outer diameter of 2.0 mm, 3.04 mm, and 7.00 mm, respectively. According to the measured electromagnetic parameters, the microwave absorbing properties of the samples can be evaluated by the reflection loss (RL), which can be calculated based on transmission line theory as follows:

$$\text{RL (dB)} = 20\lg|(Z_{\text{in}} - 1)/(Z_{\text{in}} + 1)| \quad (1)$$

$$Z_{\text{in}} = (\mu_r/\varepsilon_r)^{1/2} \tanh\left[j(2\pi fd/c)(\varepsilon_r\mu_r)^{1/2}\right], \quad (2)$$

where Z_{in} is the normalized input impedance, c is the light velocity in vacuum ($3 \times 10^8\text{ m s}^{-1}$), f is microwave frequency (Hz), d is the sample thickness (m), ε_r ($\varepsilon_r = \varepsilon' - j\varepsilon''$), and μ_r ($\mu_r = \mu' - j\mu''$) are relative complex permittivity and permeability, respectively.

4 Results and discussion

The crystal structures of the prepared Co and Co@C networks were determined by the XRD patterns as shown in Fig. 2a. It is shown that both the Co and Co@C powders exhibit three obvious characteristic peaks at around 44.22° , 51.52° , and 75.85° , which can be indexed to the (111), (200), and (220) crystal planes of the face-centered cubic metal cobalt (PDF# 15–0806), respectively. No significant characteristic peaks of carbon were found in the Co@C XRD spectrum, maybe due to the poor crystallinity of the coated carbon layer. However, the existence of the carbon in Co@C powders was certified by the Raman

spectrum as shown in Fig. 2b. It is well known that Raman spectrum is a very effective method to determine the existence of different types of carbon, and the D and G bands of Raman spectrum stand for the vibration of sp^3 atoms of disordered graphite, and the in-plane vibration of sp^2 atoms in a 2D hexagonal lattice, respectively. It is shown in Fig. 2b that both D and G bands appear at around 1350 and 1590 cm^{-1} in the Co@C spectrum, indicating the existence of the carbon layer. Meanwhile, there are no peaks in the Co spectrum, which means the corncob templates were burnt out completely in the oxidation calcination process.

Figure 2c shows the XPS spectrum of the Co@C network, which further certified the existence of carbon in the Co@C network by the obvious C 1s signal peak. O 1s signal peak was also found in the XPS spectrum. The existing O in the Co@C network can be ascribed to the residual oxygen-containing functional groups in the carbon coating process (for example, C–O and –OH as shown in Fig. 2d and Fig. S1). Compared with the sharp peaks of C 1s and O 1s, the Co 2p signal peaks in Fig. 2c are very weak. This can be explained by the limited detecting depth of XPS, and it also can be concluded that the Co network was coated by a carbon layer.

Figure 3a shows the microstructure of the corncobs, from which it can be seen that the corncobs possess a regular porous structure. Therefore, once the corncobs were immersed in $\text{Co}(\text{NO}_3)_2$ solution, Co^{2+} can be absorbed in the walls of the pores easily as shown in Fig. S2a. Figures S2b–f show the changes of the corncobs absorbed Co^{2+} at different temperatures under the oxidation calcination process. It is shown that with the increased calcination temperatures, the corncobs were first broken into pieces, and then burnt up gradually. When the temperature was increased to $700\text{ }^{\circ}\text{C}$, the corncobs were burnt out completely, and only Co_3O_4 networks were left. The Co_3O_4 can be reduced to Co by H_2 in the reduction calcination process, and Figs. 3b and c show that the reduced Co shows a structure of coralloid network. Compared with the Co network, the Co@C network possesses a thicker diameter as shown in Figs. 3d and e, due to the coated carbon layer. The core–shell structure of the Co@C was further certified by the TEM image shown in Fig. 3f, which clearly shows that the Co network was coated with a uniform carbon layer with a thickness of about 80 nm.

Fig. 2 XRD patterns **a** and Raman spectra **b** of the Co and Co@C networks, XPS spectrum **c** and the high-resolution XPS spectrum of C1s **d** of the Co@C network

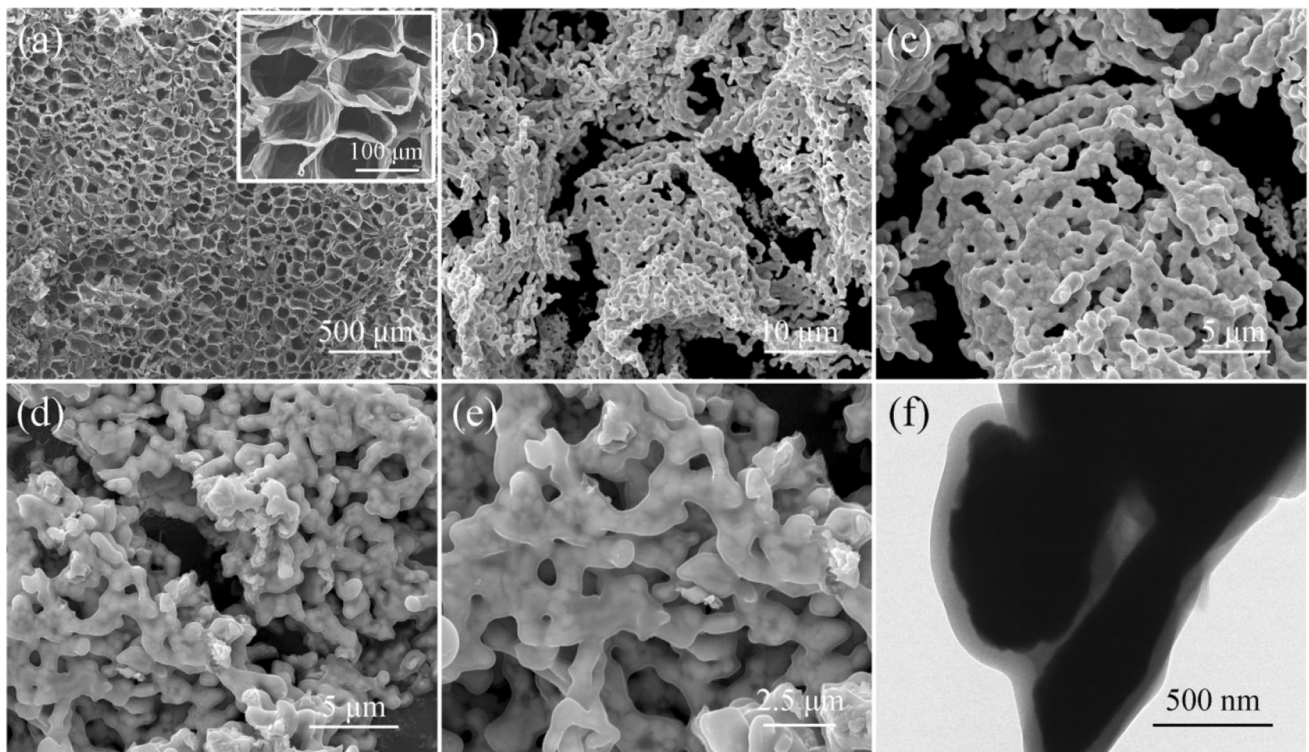
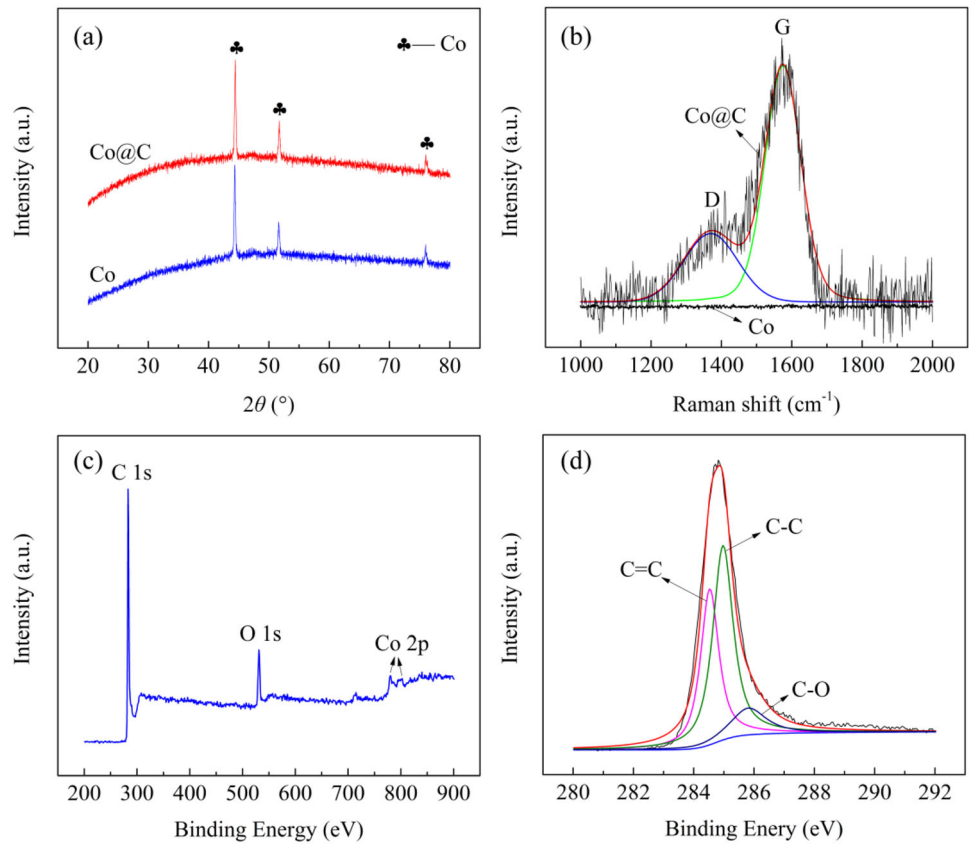


Fig. 3 SEM images of corncoabs **a**, Co network **b**, **c** and Co@C network **d**, **e**, and TEM image of the Co@C network

TG technology is an effective method to reflect the property changes of materials at different temperatures, such as phase transformation, weight loss, and thermal stability [38]. Figure 4 shows the TG curves of the Co and Co@C networks under air atmosphere. It is shown that the Co network begins to oxidize significantly at about 300 °C, and the weight increase trend to be stable at 650 °C. The total weight increase of 36.10% is very close to the theory weight change of 36.20% (from Co to Co₃O₄), which means no impurities exist in the Co network. For the Co@C network, the TG curve first shows a drastic decrease at about 300 °C, which can be ascribed to the oxidation of the coated carbon layer (from C to CO₂). And then, the curve increases in 400–650 °C, due to the oxidation of the Co network. The total weight change shows a loss of 9.68%, from which the carbon content in the Co@C composite can be calculated to be 33.7% according to Eq. (3) as follows:

$$\text{Carbon}(wt\%) = 1 - \left(\frac{1 - \text{weightloss}}{M_{\text{Co}_3\text{O}_4}} \times 3M_{\text{Co}} \right), \quad (3)$$

where *M* is the relative molecular weight of Co₃O₄ (240.8 g mol⁻¹) and Co (58.9 g mol⁻¹).

Figure 5 shows the magnetic hysteresis loops of the Co and Co@C networks measured at room temperature. Both of the two samples exhibit representative soft ferromagnetic characteristic. The saturation magnetization (*M_s*) of the Co and Co@C networks are 192 and 82 emu g⁻¹, respectively. The smaller *M_s* of Co@C is owing to the presence of the nonmagnetic carbon layer, which may be detrimental to the magnetic loss of the absorber. It is also found that the *M_s* of the Co network is higher than most of the reported Co-based materials [39–43]. Generally, the shape anisotropy of magnetic materials can influence their

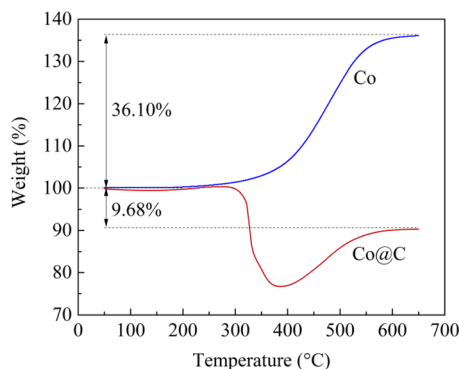


Fig. 4 TG curves of the Co and Co@C networks under air atmosphere

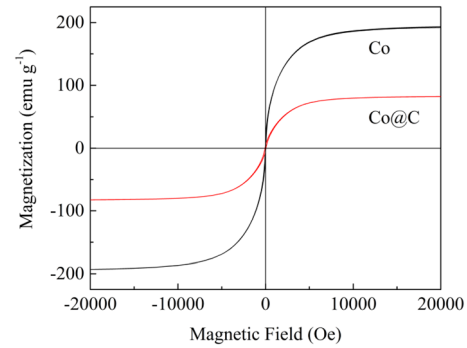
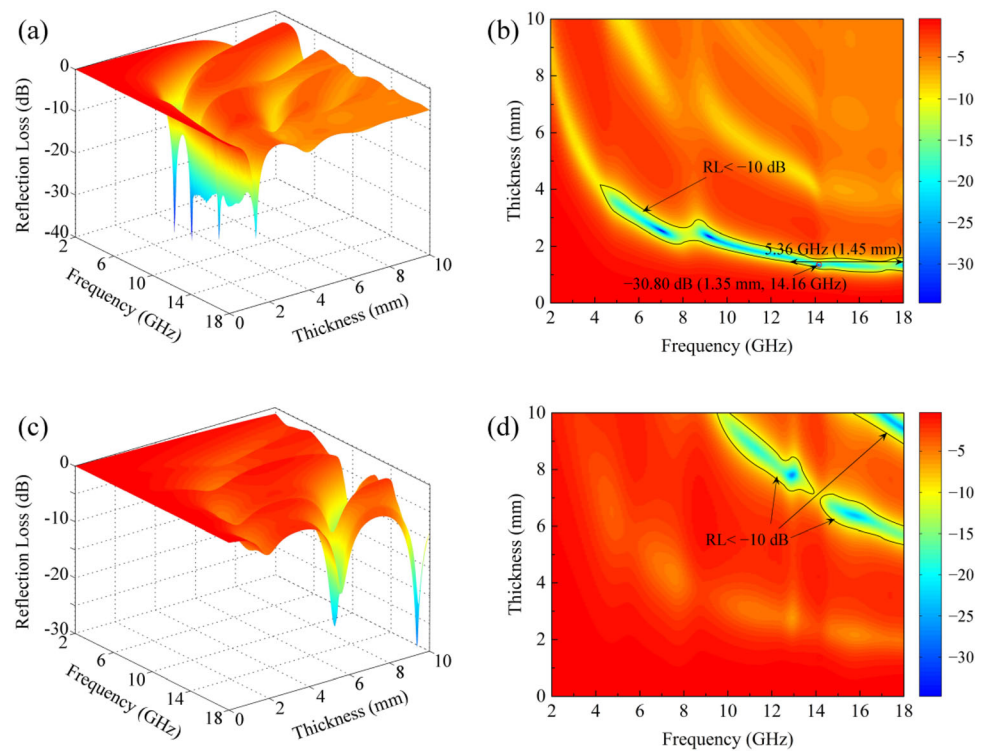


Fig. 5 Magnetic hysteresis loops of the Co and Co@C networks at room temperature

magnetization behaviors significantly, and one-dimensional (1D) morphology is beneficial to optimized magnetic parameters [23, 44]. The Co network is made up of a large number of 1D coralloid Co particles, and this maybe the reason why it possesses a very high *M_s*. The excellent magnetic property of the Co network is conducive to a strong magnetic loss.

Figures 6a and b show the three-dimensional and two-dimensional diagrams of the calculated RL values of the Co sample, respectively. It is shown that the RL value changes significantly with the variable microwave frequencies and sample thicknesses. At the sample thickness of 2.34 mm, the RL reaches up to – 54.74 dB, and the effective absorbing bandwidth (EAB, RL is less than – 10 dB, meaning more than 90% of the incident microwave was absorbed) is 3.20 GHz (the RL values in Figs. 6a and b were truncated to – 35.0 dB for clarity, and the corresponding partial enlarged detail can be found in Fig. S3). What is more, Fig. 6b exhibits that an excellent microwave absorbing property for the Co sample can be obtained just under a small sample thickness. With a sample thickness of 1.35 mm, the RL value reaches – 30.80 dB at 14.16 GHz, while at the sample thickness of 1.45 mm, the EAB is up to 5.36 GHz (12.64–18 GHz). Compared with the outstanding property of the Co sample, it is strange to find that the Co@C sample exhibits a very poor microwave absorption performance. Figures 6c and d show that for the Co@C sample, the RL value of less than – 10 dB can be obtained at some frequencies only when the sample thickness is more than 5 mm. This high thickness is almost meaningless for a microwave absorbing coating, and so the Co@C network is not appropriate as a microwave absorber.

Fig. 6 Three-dimensional and two-dimensional diagrams of the reflection losses of Co **a**, **b** and Co@C networks **c**, **d**. The minimum RL value, the largest effective bandwidth, and the regions of $RL < -10$ dB are labeled in the two-dimensional diagrams



The results of Fig. 6 indicate that the Co network possesses an excellent microwave absorbing property. However, far from optimizing the microwave absorbing property of the Co network, the coated carbon layer leads to serious performance degradation. This phenomenon appears contradictory to many reported literatures, which confirmed the positive role of the introduced carbon shell [42, 45]. In order to find out the reason of this phenomenon, the electromagnetic parameters, which directly determined the microwave absorbing properties of the samples, are analyzed in detail as follows.

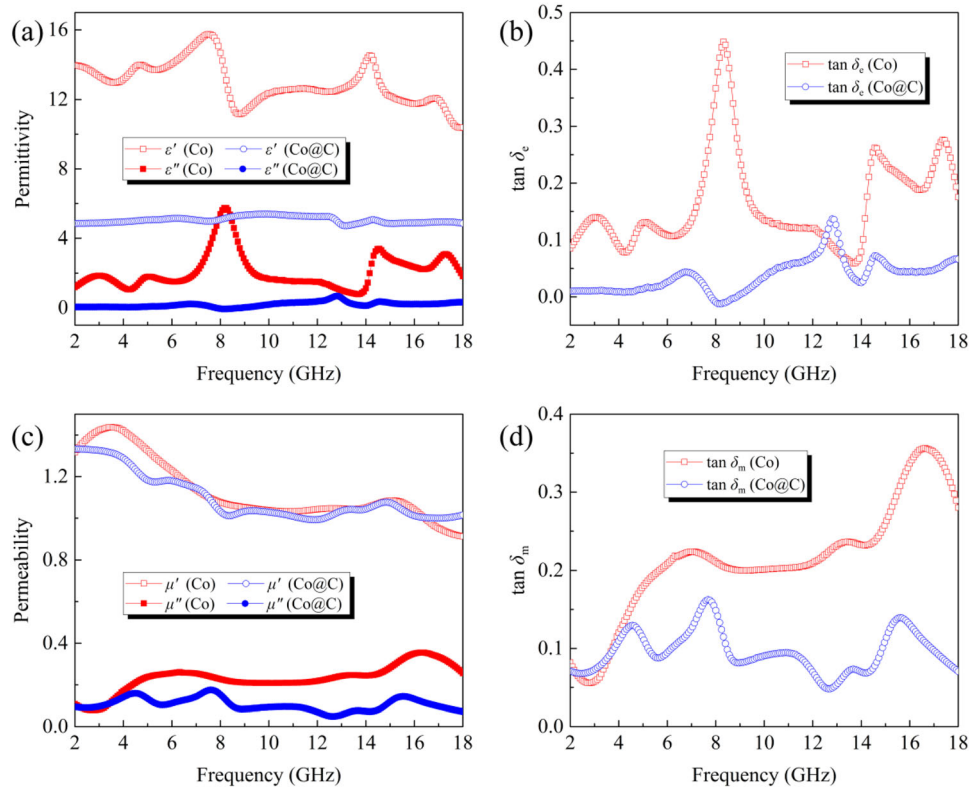
Figure 7a shows the relative complex permittivity of the Co and Co@C samples. It can be seen that both the real part (ϵ') and imaginary part (ϵ'') of the permittivity of Co sample are larger than that of Co@C sample. As we know that the real part of the electromagnetic parameter represents the energy storage, while the imaginary part stands for the energy dissipation. Therefore, the dielectric loss capacity of absorbers can be characterized by the dielectric loss factor ($\tan \delta_e = \epsilon''/\epsilon'$). Figure 7b shows the dielectric loss factors of the Co and Co@C samples, which exhibits that the Co sample has the higher dielectric loss than Co@C. Generally, the dielectric loss is from conduction loss and polarization loss. The conductivity of metal Co is better than amorphous carbon.

Therefore, the conductivity of the Co network will decrease after the carbon coating. According to the free electron theory, $\epsilon'' = \sigma/(2\pi\epsilon_0f)$ (ϵ_0 is the vacuum dielectric constant, and σ is the electric conductivity of the absorber) [46], the imaginary part of the permittivity is proportional to the conductivity. Therefore, the Co network has the higher ϵ'' and stronger conduction loss [47]. In addition, some obvious resonance peaks appear at the ϵ'' curve of the Co sample, while the ϵ'' curve of the Co@C is almost flat, which means the higher polarization loss of the Co sample. Both the stronger conduction loss and polarization loss of the Co sample lead to its higher dielectric loss factor.

Similarly, both the relative complex permeability and magnetic loss factor ($\tan \delta_m = \mu''/\mu'$) of the Co sample were reduced when the nonmagnetic carbon layer was introduced, as shown in Figs. 7c and d. This is consistent with the result of the saturation magnetization shown in Fig. 5. In addition, the magnetic loss of the Co network is higher than some other Co-based materials [39, 40]. This enhanced magnetic loss may be beneficial to stronger microwave absorption.

Besides the electromagnetic loss factors, the microwave attenuation capability of an absorber can be evaluated by the attenuation constant (α) as well,

Fig. 7 The relative complex permittivity **a**, dielectric loss factors **b**, relative complex permeability **c**, and magnetic loss factors **d** of the Co and Co@C samples



which can be calculated according to Eq. (4) as follows:

$$\alpha = \frac{\sqrt{2\pi f}}{c} \sqrt{\mu''\epsilon'' - \mu'\epsilon' + \sqrt{(\mu''\epsilon'' - \mu'\epsilon')^2 + (\epsilon'\mu'' + \epsilon''\mu'^2)}} \tag{4}$$

As shown in Fig. S4, the α value of the Co sample decreased significantly when the Co network was coated with the carbon layer. This is consistent with the electromagnetic loss factors shown in Figs. 7b and d.

Based on the above, it can be concluded that the carbon layer on the Co network caused the reduction of the ability to dissipate microwaves, due to its nonmagnetic property and lower dielectric property. However, it is still inadequate to explain the poor microwave absorbing property of the Co@C sample. Many literatures reported that the introduced carbon component can enhance the microwave absorbing property of magnetic materials, mainly by adjusting the impedance matching [48–50]. Therefore, if the introduced carbon layer can improve the impedance matching of the Co network, an enhanced microwave absorbing property can still be expected for the Co@C network. In order to characterize the impedance

matching degree, a delta-function was usually used which is described as follows [42, 51]:

$$|\Delta| = |\sinh^2(Kfd) - M| \tag{5}$$

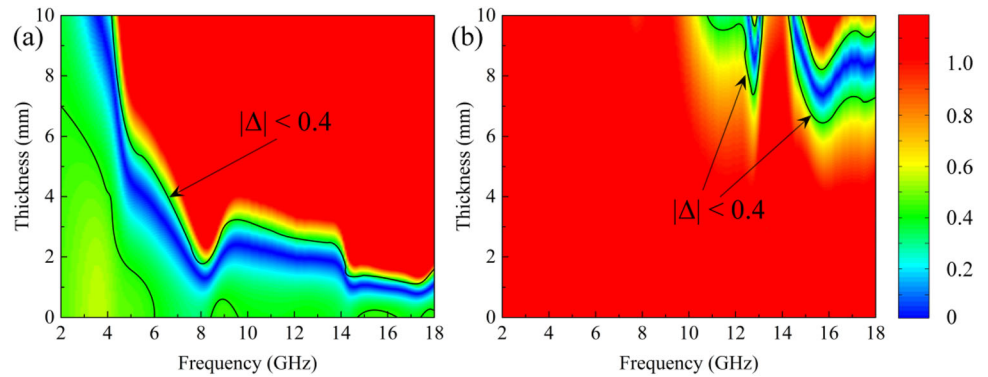
where K and M can be calculated by the following equations:

$$K = \frac{4\pi(\mu'\epsilon')^{1/2} \sin[(\delta_e + \delta_m)/2]}{c \cos\delta_e \cos\delta_m} \tag{6}$$

$$M = \frac{4\mu' \cos\delta_e \epsilon' \cos\delta_m}{(\mu' \cos\delta_e - \epsilon' \cos\delta_m)^2 + [\tan(\frac{\delta_m}{2} - \frac{\delta_e}{2})]^2 (\mu' \cos\delta_e \epsilon' \cos\delta_m)^2} \tag{7}$$

Equation (5) indicates that a smaller $|\Delta|$ value represents a better impedance matching. Generally, the $|\Delta|$ value needs to be less than 0.4 for a satisfactory impedance matching [32]. As shown in Fig. 8, the Co sample has a markedly better impedance matching than Co@C, and the Co@C sample has a small region of $|\Delta| < 0.4$ only when the sample thickness is bigger than 6 mm. This means it is not always effective to improve the impedance matching by introducing carbon component into magnetic materials. As we know, the smaller difference between dielectric loss and magnetic loss, the better

Fig. 8 Calculated $|\Delta|$ values of the Co **a** and Co@C **b** samples according to Eq. (5)



the impedance matching [52]. In general, the magnetic loss is predominant for magnetic materials. Therefore, when the carbon component is introduced, it can balance the magnetic loss and dielectric loss, by decreasing the magnetic property and keeping the dielectric property almost unchanged, and then lead to an optimized impedance matching. However, the Co network in this study can form a conductive network in the paraffin matrix, which is conducive to an enhanced dielectric loss [27, 53]. It is shown in Figs. 7b and d that the dielectric loss of the Co sample is high enough and comparable to the magnetic loss. Therefore, the Co sample itself has a good impedance matching, and the introduced carbon layer will break the balance between the dielectric loss and magnetic loss, and then lead to the poor impedance matching of the Co@C sample.

The loss mechanism of the Co network is further analyzed as follows. It is well known that the dielectric polarization loss is mainly from the polarization of space charges, dipoles, ions and electrons, in which the dipolar polarization usually plays the main role in microwave frequency band. It is shown in Fig. 7a that the ϵ'' curve of the Co sample exhibits five polarization peaks, which can be described by the Debye relaxation model as follows:

$$\epsilon(f) = \epsilon_\infty + \frac{\epsilon_s - \epsilon_\infty}{1 + j2\pi f\tau} = \epsilon'(f) + j\epsilon''(f)^2, \tag{8}$$

where ϵ_∞ , ϵ_s , and τ are relative permittivity at high frequency limit, static permittivity, and relaxation time, respectively. According to Eq. (8), the plot of ϵ' versus ϵ'' in each polarization peak should be a semicircle, i.e., the Cole–Cole semicircle, whose expression is shown as follows:

$$\left(\epsilon' - \frac{\epsilon_s + \epsilon_\infty}{2}\right)^2 + (\epsilon'')^2 = \left(\frac{\epsilon_s - \epsilon_\infty}{2}\right)^2 \tag{9}$$

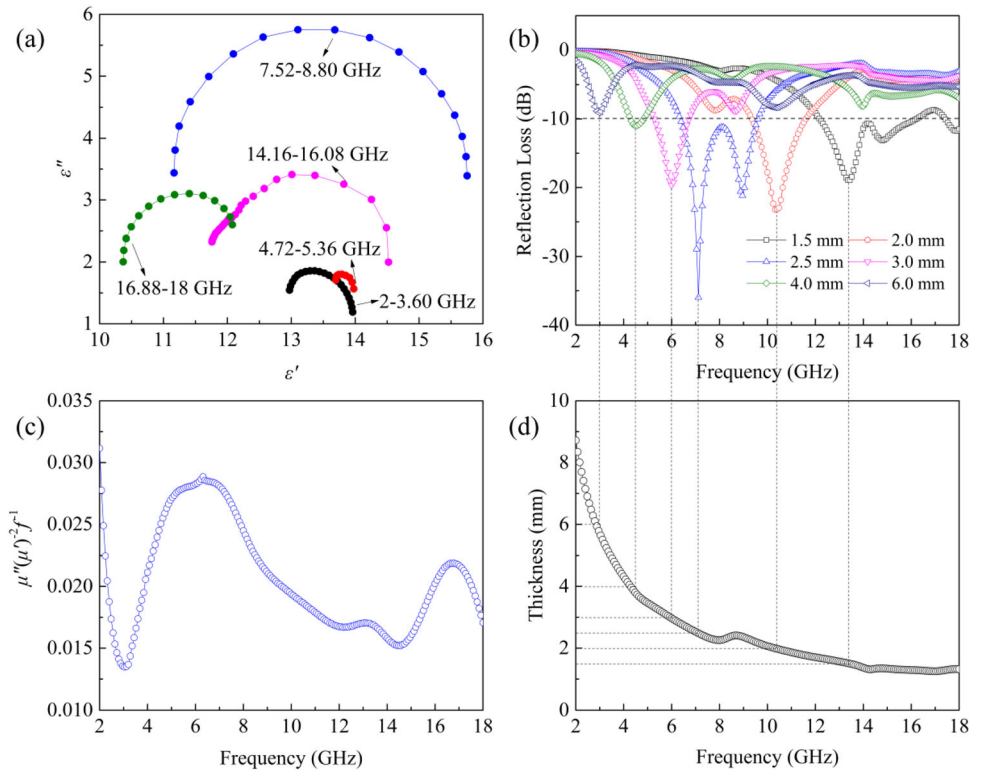
Figure 9a shows that there are five Cole–Cole semicircles for the Co network, which are totally consistent with the five polarization peaks in Fig. 7a. The five semicircles indicate that multi-dielectric relaxation processes contribute to the dielectric loss [54]. In addition, we know that for the dipolar polarization, each resonance peak of ϵ'' corresponds to a descent stage of ϵ' , and it has been confirmed as shown in Fig. S5. However, the ϵ' also shows some obvious peaks, especially at around 8 GHz, both resonance and antiresonance peaks appear. This can be ascribed to the vibration of atoms and electrons, therefore, the atomic polarization and electronic polarization may also play their roles on the dielectric loss.

The magnetic loss can be caused by magnetic hysteresis, domain-wall displacement, eddy current loss, and natural resonance, among which only the latter two are possible loss mechanism in the weak EM field and microwave frequency band. The eddy current effect can be judged by the value of $\mu''(\mu')^{-2}f^{-1}$, which should be a constant if the magnetic loss is from the eddy current effect. Therefore, it can be concluded that the magnetic loss mechanism is mainly from natural resonance, due to the drastic fluctuation of the $\mu''(\mu')^{-2}f^{-1}$ value as shown in Fig. 9c.

Figures 6b and 9b show that the minimum RL of the Co sample moves toward a lower frequency with increased thickness. This phenomenon is in line with the quarter-wavelength cancellation model as shown in Eq. (10), which shows that the t_m is inversely proportional to the f_m .

$$t_m = \frac{n\lambda}{4} = \frac{nc}{4f_m\sqrt{|\mu_r||\epsilon_r|}} (n = 1, 3, 5, \dots), \tag{10}$$

Fig. 9 The Cole–Cole semicircles **a**, reflection loss **b**, $\mu''(\mu')^{-2}f^{-1}$ value **c**, and the relationship between matching thickness and peak frequency according to the quarter-wavelength model **d** of the Co sample



where t_m and f_m are the matching thickness and matching frequency, respectively. The quarter-wavelength cancellation model reflects the interference effect of the two microwaves reflected from the upper and lower surfaces of the sample. Figure 9d displays the curve of t_m versus f_m according to Eq. (10). It is obvious that the peak frequencies at different thicknesses shown in Fig. 9b are located on the quarter-wavelength model curve, which confirms the contribution of the quarter-wavelength absorbing mechanism to the microwave absorbing property of the Co network.

The RL and EAB are the two most commonly used factors to evaluate the microwave absorbing property. However, these two factors may be not reasonable enough, because the sample thickness is not taken into consideration. The high RL and EAB may be meaningless if the sample thickness is very thick for a microwave absorbing coating. Therefore, here we present two new factors, $\alpha_{RL/d}$ ($\alpha_{RL/d} = RL/d$) and $\alpha_{EAB/d}$ ($\alpha_{EAB/d} = EAB/d$), to characterize the microwave absorbing property of the absorber in per unit thickness. As shown in Fig. 10 and Table S1, compared with most of the reported Co-based materials [15, 39–41, 43, 55–65], the Co network in this work exhibits higher $\alpha_{RL/d}$ and $\alpha_{EAB/d}$, which means

it is a good candidate for the microwave absorbing materials with strong absorption, thin thickness, wide absorbing band, and light weight. The excellent microwave absorbing property of the Co network is from the strong conduction loss, dipolar polarization, natural resonance, good impedance matching, and the quarter-wavelength absorbing mechanism.

5 Conclusions

In conclusion, the Co powder with a network structure was prepared through a simple immersion–calcination method by using corncobs as templates. Due to the enhanced dielectric loss, magnetic loss, and optimized impedance matching caused by the network structure, the Co sample exhibits an excellent microwave absorbing property. At the sample thickness of 2.34 mm, the RL reaches up to -54.74 dB, and the EAB is 3.20 GHz. What is more, the Co network shows strong and broadband absorption at small thicknesses. At the sample thickness of 1.35 mm, the RL value reaches -30.80 dB at 14.16 GHz, while the EAB is up to 5.36 GHz (12.64–18 GHz) at the sample thickness of 1.45 mm. However, unlike most of the reported magnetic

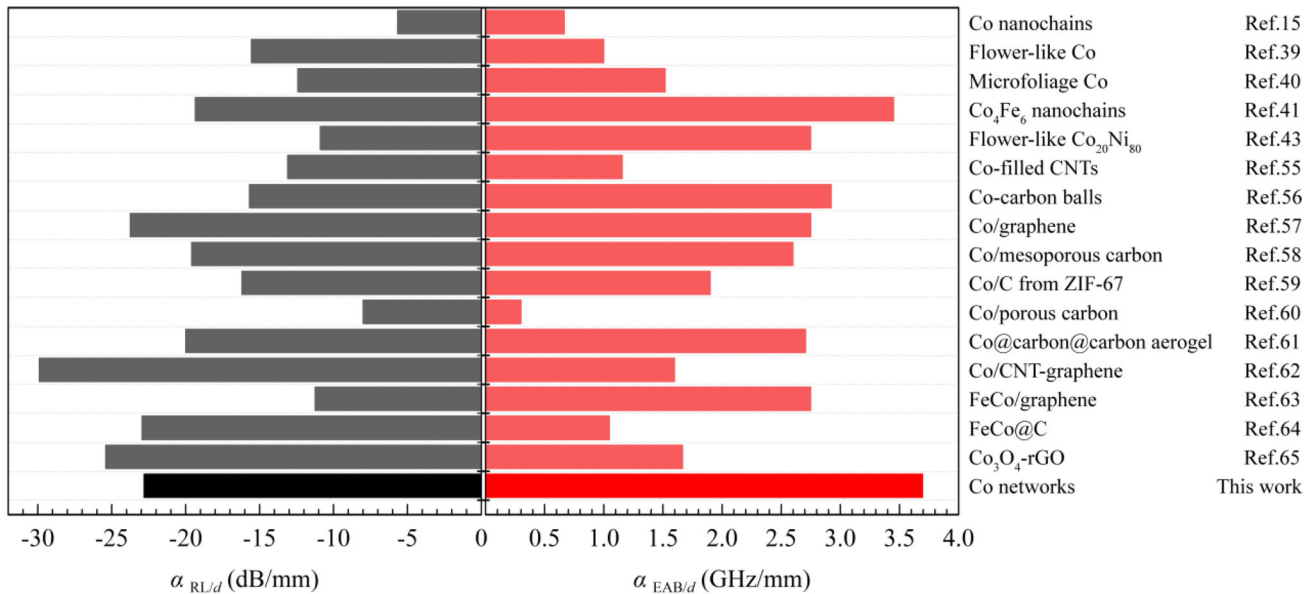


Fig. 10 Comparison of microwave absorption performance of the Co network with the reported Co-based materials

materials, the introduced carbon layer on the Co network plays a negative role, and the Co@C network shows a poor microwave absorbing property, due to the decreased loss capability and deteriorated impedance matching. Therefore, we made the Co powder a promising microwave absorber with strong absorption, wide absorbing band, and thin thickness just by constructing a network structure, without needing extra carbon decorating.

Acknowledgements

This work was supported by the National Natural Science Foundation of China [grant number 51604005], and the Open Fund of Anhui Province Key Laboratory of Metallurgy Engineering & Resources Recycling [grant number SKF19-01].

Funding

This work was supported by the National Natural Science Foundation of China [grant number 51604005], and the Open Fund of Anhui Province Key Laboratory of Metallurgy Engineering & Resources Recycling [grant number SKF19-01].

Data Availability

All data generated or analyzed during this study are included in this published article (and its supplementary information files).

Declarations

Conflict of interest The authors declare that they have no competing interests.

Supplementary Information: The online version contains supplementary material available at <http://doi.org/10.1007/s10854-021-07240-3>.

References

1. Y. Sun, P. Ni, M. Zhu, Y. Yao, S. Fu, Preparation of Fe₃O₄@C submicron rods for adsorption of methylene blue and fast separation from water. *Micro Nano Lett.* **14**, 962–966 (2019). <https://doi.org/10.1049/mnl.2019.0111>
2. X. Cui, Q. Yang, L. Yang, R. Krishna, Z. Zhang, Z. Bao, H. Wu, Q. Ren, W. Zhou, B. Chen, Ultrahigh and selective SO₂ uptake in inorganic anion-pillared hybrid porous materials. *Adv. Mater.* **29**, 1606929 (2017). <https://doi.org/10.1002/adma.201606929>
3. Y. Yao, M. Zhu, Z. Zhao, B. Tong, Y. Fan, Z. Hua, Hydrometallurgical processes for recycling spent lithium-ion batteries: A critical review. *ACS Sustainable Chem. Eng.* **6**,

- 13611–13627 (2018). <https://doi.org/10.1021/acssuschemeng.8b03545>
4. Y. Sun, M. Zhu, Y. Yao, H. Wang, B. Tong, Z. Zhao, A novel approach for the selective extraction of Li^+ from the leaching solution of spent lithium-ion batteries using benzo-15-crown-5 ether as extractant. *Sep. Purif. Technol.* **237**, 116325 (2020). <https://doi.org/10.1016/j.seppur.2019.116325>
 5. G. Fang, C. Liu, Y. Yang, Y. Lin, M. Xu, K. Peng, Y. Zhang, Y. Cao, Z. Liu, Y. Zhang, Enhanced microwave absorption performance of $\text{Fe}_3\text{O}_4/\text{Cu}$ composites with coexistence of nanospheres and nanorods. *J. Alloys Compd.* **817**, 152764 (2020). <https://doi.org/10.1016/j.jallcom.2019.152764>
 6. X. Meng, S. Dong, Design and construction of lightweight C/Co heterojunction nanofibres for enhanced microwave absorption performance. *J. Alloys Compd.* **810**, 151806 (2019). <https://doi.org/10.1016/j.jallcom.2019.151806>
 7. L.J. Yu, Q.X. Yang, J.L. Liao, Y.F. Zhu, X. Li, W.T. Yang, Y.Q. Fu, A novel 3D silver nanowires@polypyrrole sponge loaded with water giving excellent microwave absorption properties. *Chem. Eng. J.* **352**, 490–500 (2018). <https://doi.org/10.1016/j.cej.2018.07.047>
 8. Z. Lou, Y. Li, H. Han, H. Ma, L. Wang, J. Cai, L. Yang, C. Yuan, J. Zou, Synthesis of porous 3D Fe/C composites from waste wood with tunable and excellent electromagnetic wave absorption performance. *ACS Sustainable Chem. Eng.* **6**, 15598–15607 (2018). <https://doi.org/10.1021/acssuschemeng.8b04045>
 9. G. Kulkarni, P. Kandesar, N. Velhal, V. Phadtare, A. Jatrakar, S.K. Shinde, D.Y. Kim, V. Puri, Exceptional electromagnetic interference shielding and microwave absorption properties of room temperature synthesized polythiophene thin films with double negative characteristics (DNG) in the Ku-band region. *Chem. Eng. J.* **355**, 196–207 (2019). <https://doi.org/10.1016/j.cej.2018.08.114>
 10. M. Zhang, H. Ling, S. Ding, Y. Xie, T. Cheng, L. Zhao, T. Wang, H. Bian, H. Lin, Z. Li, A. Meng, Synthesis of CF@PANI hybrid nanocomposites decorated with Fe_3O_4 nanoparticles towards excellent lightweight microwave absorber. *Carbon* **174**, 248–259 (2021). <https://doi.org/10.1016/j.carbon.2020.12.005>
 11. B. Quan, W. Gu, J. Sheng, X. Lv, Y. Mao, L. Liu, X. Huang, Z. Tian, G. Ji, From intrinsic dielectric loss to geometry patterns: Dual-principles strategy for ultrabroad band microwave absorption. *Nano Res.* **14**(5), 1495–1501 (2021). <https://doi.org/10.1007/s12274-020-3208-8>
 12. H. Lv, G. Ji, M. Wang, C. Shang, H. Zhang, Y. Du, Hexagonal-cone like of $\text{Fe}_{50}\text{Co}_{50}$ with broad frequency microwave absorption: Effect of ultrasonic irradiation time. *J. Alloys Compd.* **615**, 1037–1042 (2014). <https://doi.org/10.1016/j.jallcom.2014.07.118>
 13. P. Yang, H. Ruan, Y. Sun, R. Li, Y. Lu, C. Xiang, Excellent microwave absorption performances of high length-diameter ratio iron nanowires with low filling ratio. *Nanotechnology* **31**, 395708 (2020). <https://doi.org/10.1088/1361-6528/ab9d41>
 14. J. Kong, F.L. Wang, X.Z. Wan, J.R. Liu, M. Itoh, K. Machida, Template-free synthesis of Co nanoporous structures and their electromagnetic wave absorption properties. *Mater. Lett.* **78**, 69–71 (2012). <https://doi.org/10.1016/j.matlet.2012.03.026>
 15. X.-L. Shi, M.-S. Cao, J. Yuan, X.-Y. Fang, Dual nonlinear dielectric resonance and nesting microwave absorption peaks of hollow cobalt nanochains composites with negative permeability. *Appl. Phys. Lett.* **95**, 163108 (2009). <https://doi.org/10.1063/1.3250170>
 16. C. Zhang, Y. Yao, J. Zhan, J. Wu, C. Li, Template-free synthesis of Ni microfibres and their electromagnetic wave absorbing properties. *J. Phys. D: Appl. Phys.* **46**, 495308 (2013). <https://doi.org/10.1088/0022-3727/46/49/495308>
 17. Y. Yao, C. Zhang, Y. Fan, J. Zhan, Preparation and microwave absorbing property of porous FeNi powders. *Adv. Powder Technol.* **27**, 2285–2290 (2016). <https://doi.org/10.1016/j.apt.2016.08.022>
 18. J. Feng, Y. Zong, Y. Sun, Y. Zhang, X. Yang, G. Long, Y. Wang, X. Li, X. Zheng, Optimization of porous $\text{FeNi}_3/\text{N-GN}$ composites with superior microwave absorption performance. *Chem. Eng. J.* **345**, 441–451 (2018). <https://doi.org/10.1016/j.cej.2018.04.006>
 19. S. Bergeul, F. Otmane, M. Azzaz, Structural and microwave absorption properties of nanostructured Fe-Co alloys. *Adv. Powder Technol.* **23**, 580–582 (2012). <https://doi.org/10.1016/j.apt.2011.06.004>
 20. Y. Cheng, G. Ji, Z. Li, H. Lv, W. Liu, Y. Zhao, J. Cao, Y. Du, Facile synthesis of FeCo alloys with excellent microwave absorption in the whole Ku-band: Effect of Fe/Co atomic ratio. *J. Alloys Compd.* **704**, 289–295 (2017). <https://doi.org/10.1016/j.jallcom.2017.02.024>
 21. B. Wang, C. Zhang, C. Mu, R. Yang, J. Xiang, J. Song, F. Wen, Z. Liu, Enhanced electromagnetic wave absorption properties of NiCo_2 nanoparticles interspersed with carbon nanotubes. *J. Magn. Magn. Mater.* **471**, 185–191 (2019). <https://doi.org/10.1016/j.jmmm.2018.09.090>
 22. Y. Yao, M. Zhu, C. Zhang, Y. Fan, J. Zhan, Effects of composition on the microwave absorbing properties of $\text{Fe}_x\text{Ni}_{100-x}$ ($x = 0-25$) submicro fibers. *Adv. Powder Technol.* **29**, 1099–1105 (2018). <https://doi.org/10.1016/j.apt.2018.01.028>
 23. Y. Yao, C. Zhang, Y. Fan, J. Zhan, Preparation of $\text{Fe}_{20}\text{Ni}_{80}$ submicron fibers by an oxalate precipitation-thermal decomposition process and their microwave absorbing properties. *J. Mater. Sci.: Mater. Electron.* **28**, 13548–13555 (2017). <https://doi.org/10.1007/s10854-017-7194-x>

24. Z.C. Lou, C.L. Yuan, Y. Zhang, Y.J. Li, J.B. Cai, L.T. Yang, W.K. Wang, H. Han, J. Zou, Synthesis of porous carbon matrix with inlaid $\text{Fe}_3\text{C}/\text{Fe}_3\text{O}_4$ micro-particles as an effective electromagnetic wave absorber from natural wood shavings. *J. Alloys Compd.* **775**, 800–809 (2019). <https://doi.org/10.1016/j.jallcom.2018.10.213>
25. Y. Fan, Y. Li, Y. Yao, Y. Sun, B. Tong, J. Zhan, Hierarchically porous carbon sheets/Co nanofibers derived from corncobs for enhanced microwave absorbing properties. *Appl. Surf. Sci.* **534**, 147510 (2020). <https://doi.org/10.1016/j.apsusc.2020.147510>
26. Y. Wang, X. Di, X. Gao, X. Wu, Design of MOF-derived hierarchical $\text{Co}@C@RGO$ composite with controllable heterogeneous interfaces as a high-efficiency microwave absorbent. *Nanotechnology* **31**, 395710 (2020). <https://doi.org/10.1088/1361-6528/ab97d1>
27. W. Gu, J. Sheng, Q. Huang, G. Wang, J. Chen, G. Ji, Environmentally friendly and multifunctional shaddock peel-based carbon aerogel for thermal-insulation and microwave absorption. *Nano-Micro Lett.* **13**, 102 (2021). <https://doi.org/10.1007/s40820-021-00635-1>
28. P.B. Liu, Y.Q. Zhang, J. Yan, Y. Huang, L. Xia, Z.X. Guang, Synthesis of lightweight N-doped graphene foams with open reticular structure for high-efficiency electromagnetic wave absorption. *Chem. Eng. J.* **368**, 285–298 (2019). <https://doi.org/10.1016/j.ccej.2019.02.193>
29. Z. Wu, W. Hu, T. Huang, P. Lan, K. Tian, F. Xie, L. Li, Hierarchically porous carbons with controlled structures for efficient microwave absorption. *J. Mater. Chem. C* **6**, 8839–8845 (2018). <https://doi.org/10.1039/c8tc01813h>
30. H. Zhao, Y. Cheng, Z. Zhang, B. Zhang, C. Pei, F. Fan, G. Ji, Biomass-derived graphene-like porous carbon nanosheets towards ultralight microwave absorption and excellent thermal infrared properties. *Carbon* **173**, 501–511 (2021). <https://doi.org/10.1016/j.carbon.2020.11.035>
31. P.B. Liu, S. Gao, Y. Wang, Y. Huang, J.H. Luo, Core-shell $\text{CoNi}@$ graphitic carbon decorated on B, N-codoped hollow carbon polyhedrons toward lightweight and high-efficiency microwave attenuation. *ACS Appl. Mat. Interfaces* **11**, 25624–25635 (2019). <https://doi.org/10.1021/acsami.9b08525>
32. W. Gu, X. Cui, J. Zheng, J. Yu, Y. Zhao, G. Ji, Heterostructure design of Fe_3N alloy/porous carbon nanosheet composites for efficient microwave attenuation. *J. Mater. Sci. Technol.* **67**, 265–272 (2021). <https://doi.org/10.1016/j.jmst.2020.06.054>
33. Z. Li, H. Lin, S. Ding, H. Ling, T. Wang, Z. Miao, M. Zhang, A. Meng, Q. Li, Synthesis and enhanced electromagnetic wave absorption performances of $\text{Fe}_3\text{O}_4@C$ decorated walnut shell-derived porous carbon. *Carbon* **167**, 148–159 (2020). <https://doi.org/10.1016/j.carbon.2020.05.070>
34. Y. Zhao, H. Zhang, T. Cong, H. Huang, J. Muhammad, X. Zuo, Y. Guo, L. Pan (2020) Crystallization-and morphology-tunable $\text{Fe}_3\text{O}_4@C$ core-shell composites decorated on carbon nanotube skeleton with tailorable electromagnetic wave absorption behavior. *Appl. Phys. Express* **13**, 125501. <https://doi.org/10.35848/1882-0786/abc491>.
35. Y. Zhao, H. Zhang, X. Yang, H. Huang, G. Zhao, T. Cong, X. Zuo, Z. fan, S. Yang, L. Pan, In situ construction of hierarchical core-shell $\text{Fe}_3\text{O}_4@C$ nanoparticles-helical carbon nanocoil hybrid composites for highly efficient electromagnetic wave absorption. *Carbon* **171**, 395–408 (2020). <https://doi.org/10.1016/j.carbon.2020.09.036>
36. M. Zhang, Z. Shi, J. Zhang, K. Zhang, L. Lei, D. Dastan, B. Dong, Greatly enhanced dielectric charge storage capabilities of layered polymer composites incorporated with low loading fractions of ultrathin amorphous iron phosphate nanosheets. *J. Mater. Chem. C* **9**, 10414–10424 (2021). <https://doi.org/10.1039/d1tc01974k>
37. P. Yin, Z. Shi, L. Sun, P. Xie, D. Dastan, K. Sun, R. Fan, Improved breakdown strengths and energy storage properties of polyimide composites: The effect of internal interfaces of C/SiO_2 hybrid nanoparticles. *Polym. Compos.* **42**, 3000–3010 (2021). <https://doi.org/10.1002/pc.26034>
38. Y. Jiao, Z. Huang, W. Hu, X. Li, Q. Yu, Y. Wang, Y. Zhou, D. Dastan, In-situ hybrid Cr_3C_2 and $\gamma\text{-Ni}_3(\text{Al}, \text{Cr})$ strengthened Ni matrix composites: Microstructure and enhanced properties. *Mater. Sci. Eng. A* **820**, 141524 (2021). <https://doi.org/10.1016/j.msea.2021.141524>
39. X.-J. Zhang, G.-C. Lv, G.-S. Wang, T.-Y. Bai, J.-K. Qu, X.-F. Liu, P.-G. Yin, High-performance microwave absorption of flexible nanocomposites based on flower-like Co superstructures and polyvinylidene fluoride. *RSC Adv.* **5**, 55468–55473 (2015). <https://doi.org/10.1039/c5ra06597f>
40. R. Kuchi, V. Dongquoc, D. Kim, S.-G. Yoon, S.-Y. Park, J.-R. Jeong, Large-scale room-temperature aqueous synthesis of Co superstructures with controlled morphology, and their application to electromagnetic wave absorption. *Met. Mater. Int.* **23**, 405–411 (2017). <https://doi.org/10.1007/s12540-017-6456-8>
41. Q. Jiang, H. Li, Z. Cao, H. Li, Q. Wang, Z. Jiang, Q. Kuang, Z. Xie, Synthesis and enhanced electromagnetic wave absorption performance of amorphous $\text{Co}_x\text{Fe}_{10-x}$ alloys. *J. Alloys Compd.* **726**, 1255–1261 (2017). <https://doi.org/10.1016/j.jallcom.2017.08.066>
42. D. Ding, Y. Wang, X. Li, R. Qiang, P. Xu, W. Chu, X. Han, Y. Du, Rational design of core-shell $\text{Co}@C$ microspheres for high-performance microwave absorption. *Carbon* **111**,

- 722–732 (2017). <https://doi.org/10.1016/j.carbon.2016.10.059>
43. Q. Liu, X. Xu, W. Xia, R. Che, C. Chen, Q. Cao, J. He, Dependency of magnetic microwave absorption on surface architecture of Co₂₀Ni₈₀ hierarchical structures studied by electron holography. *Nanoscale* **7**, 1736–1743 (2015). <http://doi.org/10.1039/c4nr05547k>
44. J. Lv, X.H. Liang, G.B. Ji, B. Quan, W. Liu, Y.W. Du, Structural and carbonized design of 1D FeNi/C nanofibers with conductive network to optimize electromagnetic parameters and absorption abilities. *ACS Sustainable Chem. Eng.* **6**, 7239–7249 (2018). <https://doi.org/10.1021/acssuschemeng.7b03807>
45. N. Wu, X. Liu, C. Zhao, C. Cui, A. Xia, Effects of particle size on the magnetic and microwave absorption properties of carbon-coated nickel nanocapsules. *J. Alloys Compd.* **656**, 628–634 (2016). <https://doi.org/10.1016/j.jallcom.2015.10.027>
46. D. Micheli, C. Apollo, R. Pastore, M. Marchetti, X-Band microwave characterization of carbon-based nanocomposite material, absorption capability comparison and RAS design simulation. *Compos. Sci. Technol.* **70**, 400–409 (2010). <http://doi.org/10.1016/j.compscitech.2009.11.015>
47. J. Li, D. Zhang, H. Qi, G.M. Wang, J.M. Tang, G. Tian, A.H. Liu, H.J. Yue, Y. Yu, S.H. Feng, Economical synthesis of composites of FeNi alloy nanoparticles evenly dispersed in two-dimensional reduced graphene oxide as thin and effective electromagnetic wave absorbers. *RSC Adv.* **8**, 8393–8401 (2018). <https://doi.org/10.1039/c7ra13737k>
48. B. Quan, G.Y. Xu, W.H. Gu, J.Q. Sheng, G.B. Ji, Cobalt nanoparticles embedded nitrogen-doped porous graphitized carbon composites with enhanced microwave absorption performance. *J. Colloid Interface Sci.* **533**, 297–303 (2019). <https://doi.org/10.1016/j.jcis.2018.08.083>
49. X. Gao, K. Zhang, Q. Zhang, C. Li, Y. Wang, X. Chen, Porous corn-like Fe₃O₄ nanosheets decorated fluffy graphene nanocomposites and their enhanced microwave absorption properties. *J. Mater. Sci.: Mater. Electron.* **29**, 12178–12186 (2018). <https://doi.org/10.1007/s10854-018-9326-3>
50. F.F. Yan, Y. Zong, C.J. Zhao, G.G. Tan, Y. Sun, X.H. Li, Z.Y. Ren, X.L. Zheng, Porous Co nanospheres supported on nitrogen-doped graphene as high-efficiency electromagnetic wave absorbers with thin thickness. *J. Alloys Compd.* **742**, 928–936 (2018). <https://doi.org/10.1016/j.jallcom.2018.01.388>
51. Z. Ma, Y. Zhang, C. Cao, J. Yuan, Q. Liu, J. Wang, Attractive microwave absorption and the impedance match effect in zinc oxide and carbonyl iron composite. *Physica B* **406**, 4620–4624 (2011). <https://doi.org/10.1016/j.physb.2011.09.039>
52. Q. Liao, M. He, Y.M. Zhou, S.X. Nie, Y.J. Wang, S. Hu, H.Y. Yang, H.F. Li, Y. Tong, Highly cuboid-shaped hetero-bimetallic metal-organic frameworks derived from porous Co/ZnO/C microrods with improved electromagnetic wave absorption capabilities. *ACS Appl. Mat. Interfaces* **10**, 29136–29144 (2018). <https://doi.org/10.1021/acsami.8b09093>
53. H.X. Pan, X.W. Yin, J.M. Xue, L.F. Cheng, L.T. Zhang, In-situ synthesis of hierarchically porous and polycrystalline carbon nanowires with excellent microwave absorption performance. *Carbon* **107**, 36–45 (2016). <https://doi.org/10.1016/j.carbon.2016.05.045>
54. S. Wei, Z. Shi, W. Wei, H. Wang, D. Dastan, M. Huang, J. Shi, S. Chen, Facile preparation of ultralight porous carbon hollow nanoboxes for electromagnetic wave absorption. *Ceram. Int.* **47**, 28014–28020 (2021). <https://doi.org/10.1016/j.ceramint.2021.06.132>
55. H. Lin, H. Zhu, H. Guo, L. Yu, Microwave-absorbing properties of Co-filled carbon nanotubes. *Mater. Res. Bull.* **43**, 2697–2702 (2008). <https://doi.org/10.1016/j.materresbull.2007.10.016>
56. G. Li, L. Wang, W. Li, Y. Xu, Fe-, Co-, and Ni-loaded porous activated carbon balls as lightweight microwave absorbers. *ChemPhysChem* **16**, 3458–3467 (2015). <https://doi.org/10.1002/cphc.201500608>
57. G. Pan, J. Zhu, S. Ma, G. Sun, X. Yang, Enhancing the electromagnetic performance of Co through the phase-controlled synthesis of hexagonal and cubic Co nanocrystals grown on graphene. *ACS Appl. Mat. Interfaces* **5**, 12716–12724 (2013). <https://doi.org/10.1021/am404117v>
58. G. Shen, Y. Xu, B. Liu, P. Du, Y. Li, J. Zhu, D. Zhang, Enhanced microwave absorption properties of N-doped ordered mesoporous carbon plated with metal Co. *J. Alloys Compd.* **680**, 553–559 (2016). <https://doi.org/10.1016/j.jallcom.2016.04.181>
59. R. Qiang, Y. Du, D. Chen, W. Ma, Y. Wang, P. Xu, J. Ma, H. Zhao, X. Han, Electromagnetic functionalized Co/C composites by in situ pyrolysis of metal-organic frameworks (ZIF-67). *J. Alloys Compd.* **681**, 384–393 (2016). <https://doi.org/10.1016/j.jallcom.2016.04.225>
60. Q. Liu, D. Zhang, T. Fan, Electromagnetic wave absorption properties of porous carbon/Co nanocomposites. *Appl. Phys. Lett.* **93**, 013110 (2008). <https://doi.org/10.1063/1.2957035>
61. H.B. Zhao, J.B. Cheng, Y.Z. Wang, Biomass-derived Co@crystalline carbon@carbon aerogel composite with enhanced thermal stability and strong microwave absorption performance. *J. Alloys Compd.* **736**, 71–79 (2018). <https://doi.org/10.1016/j.jallcom.2017.11.120>
62. X. Qi, Q. Hu, J. Xu, R. Xie, Y. Jiang, W. Zhong, Y. Du, The synthesis and excellent electromagnetic radiation absorption

- properties of core/shell-structured Co/carbon nanotube–graphene nanocomposites. *RSC Adv.* **6**, 11382–11387 (2016). <https://doi.org/10.1039/c5ra24599k>
63. X. Li, J. Feng, Y. Du, J. Bai, H. Fan, H. Zhang, Y. Peng, F. Li, One-pot synthesis of CoFe_2O_4 /graphene oxide hybrids and their conversion into FeCo/graphene hybrids for lightweight and highly efficient microwave absorber. *J. Mater. Chem. A* **3**, 5535–5546 (2015). <https://doi.org/10.1039/c4ta05718j>
64. Y. Zhang, P. Wang, Y. Wang, L. Qiao, T. Wang, F. Li, Synthesis and excellent electromagnetic wave absorption properties of parallel aligned FeCo@C core–shell nanoflake composites. *J. Mater. Chem. C* **3**, 10813–10818 (2015). <https://doi.org/10.1039/c5tc02146d>
65. J.R. Ma, X.X. Wang, W.Q. Cao, C. Han, H.J. Yang, J. Yuan, M.S. Cao, A facile fabrication and highly tunable microwave absorption of 3D flower-like Co_3O_4 -rGO hybrid-architectures. *Chem. Eng. J.* **339**, 487–498 (2018). <https://doi.org/10.1016/j.cej.2018.01.152>

Publisher's Note Springer Nature remains neutral with regard to jurisdictional claims in published maps and institutional affiliations.